X-Ray Microbeam Laue Pattern Studies of the Spreading of Orientation in OFHC Copper at Large Strains

G. C. Butler

S. R. Stock

R. D. McGinty

D. L. McDowell

Georgia Institute of Technology, Atlanta, GA 30332-0245

This paper assesses, via X-ray microbeam diffraction, the effects of development of dislocation substructure on the distribution of sub-grain misorientations in annealed OFHC copper deformed to large strains for compression, for shear, and for sequences of compression followed by shear. Polychromatic synchrotron x-radiation was used to study samples from four strain histories: virgin specimens, 50% effective strain in compression, 100% effective strain in torsion, and 50% compressive strain followed by 50% torsion. A very narrow beam illuminated an approximately 15 μm diameter column through the sample, and the microstructure of the specimens was mapped by translating the sample along two orthogonal axes perpendicular to the beam by increments of 10 μm. The beam diameter was considerably smaller than the average grain size in the virgin material. Both the degree of substructure formation and the nature of the distributed microstructure were quantified from the resulting Laue diffraction patterns. The polychromatic diffraction patterns of the polycrystalline samples consisted of well-defined streaks, and the azimuthal angular width of the streaks increased with plastic strain in a manner consistent with the scaling of the misorientation distribution of high angle boundaries for sub-grains reported recently using electron microscopy techniques limited to thin foils or thin surface layers. A lattice spin correction is introduced based on this scaling law in a simple extended Taylor scheme of polycrystal plasticity to achieve a retardation of texture development that is consistent with experimental results. [DOI: 10.1115/1.1421050]

1 Introduction

The formation of deformation bands in bcc and fcc metal crystals deformed to large plastic strain levels has been a subject of considerable recent interest [1–9]. Results from transmission electron microscopy (TEM) and scanning electron microscopy (SEM) electron backscattering techniques have led to an understanding that these deformation bands are quite complex in nature, and have the following attributes, summarized from Kuhlmann-Wilsdorf et al. [9]:

- These bands' spacing refines as deformation proceeds up to equivalent strain levels of 200–300%.
- Only a limited (e.g., 2–3) number of slip systems need to be active within each band, less than the number ostensibly required of a single crystal to maintain compatibility; clusters of bands act together to fulfill the Taylor criterion.
- The measured misorientation of adjacent bands suggests the presence of high angle (>5–10 deg) boundaries, and dislocation content within these boundaries represents substantial populations of geometrically necessary dislocations needed to accommodate the misfit associated with slip incompatibility between neighboring bands.
- Individual bands do not extend across grains, but similarly oriented bands are observed in various grains.
- Deformation bands give rise to a distribution of subgrain misorientations as well as to various texture components that differ from the Taylor criterion applied to the initial grains.
- Initial formation of low angle boundaries (sometimes termed ''incidental boundaries'' or IBs) is manifested by dislocation cell wall boundaries arising from mutual trapping of glide dislocations. These may eventually give rise to development of high angle geometrically necessary boundaries (GNBs) between deformation bands at higher strains.
- Deformation bands occur more readily and are initially wider in larger grains, with profuse formation of secondary and tertiary bands within primary bands accounting for observed refinement.
- Deformation bands are less prevalent for precipitate-containing alloys at room temperature (internal stress fields of coherent precipitates tend to randomize the deformation substructures), and also at higher temperatures where statistical fluctuations of dislocation activity and orientation become more prevalent.
- Deformation bands play a role in the dependence of recrystallization and grain refinement on prior cold work.

While the TEM and SEM work has been illuminating in many respects, these techniques are based on either very thin foils/slices or on very shallow surface interrogation of the samples. Prior work has not considered sampling significant volumes of material with fairly high (sub-grain) resolution as would be accessible through high energy polychromatic synchrotron x-ray microbeams which can have a diameter substantially smaller than the mean grain size.

In this paper, subgrain-scale microtexture of polycrystalline pure Cu is investigated based on analyses of transmission Laue diffraction patterns obtained using polychromatic synchrotron X-ray microbeams. The amount and character of grain subdivision is quantified for four samples of copper, with von Mises equivalent strain levels of 50% and 100% (both monotonic and complex strain histories), and an annealed, undeformed sample. The key to the analysis is the recognition that each grain irradiated by the polychromatic beam produces a pattern of diffraction ''spots,'' the arrangement of which depends on the grain's orientation relative to the beam; this arrangement degrades to streaks as the deformation levels increase. Because each region of a subdivided crystal will form a different, slightly rotated pattern, analysis is relatively

Contributed by the Materials Division for publication in the JOURNAL OF ENGINEERING MATERIALS AND TECHNOLOGY. Manuscript received by the Materials Division October 10, 2000; revised manuscript received May 10, 2001. Guest Editors: Mohammed Cherkaoui and László S. Tóth.

straightforward, and one expects that greater amounts of subdivision in a crystal will produce a more complex Laue pattern. Different approaches can be used for x-ray microdiffraction materials analysis [10–14], and it is interesting to consider how the volumetric x-ray methods may complement or even compete with electron-based orientation mapping techniques for determining misorientation distribution at large strains.

2 Experiments

The material used in this study was annealed oxygen free high conductivity (OFHC) copper with an equiaxed grain structure and an initial grain size of approximately 60–65 μm [15]. Samples were cut from as-received material, and from material subjected to equivalent von Mises strain levels of 50% compression, 100% torsion, and 50% compression followed by 50% torsion. Pole figures from the (111), (200), and (220) planes were measured from all four samples, and these results are reported elsewhere [16]. The observed macrotextures of the samples subjected to monotonic deformation were consistent with those reported in the literature; the authors are not aware of data with which the sample with complex deformation history (50% compression followed by 50% torsion) could be compared.

Planar sections of each of these samples were cut with a slow-speed diamond wheel and hand ground from 1 mm thick sections into thin wedges. The samples were then metallographically polished on SiC paper and etched to remove polishing damage. The final thickness of the samples subjected to microbeam analysis was between 100 μm and 200 μm.

Diffraction data were collected at the Stanford Synchrotron Radiation Laboratory (SSRL) under storage ring energy of 3.0 GeV and beam currents between 50 mA and 100 mA. Both the sample and the image storage plate were normal to the incident beam. Microbeam diffraction was initially performed with a 10 μm diameter pinhole collimator placed 55 cm from the sample. However, it was determined that the beam had approximately 20 arcseconds of vertical divergence, which was enough to broaden the beam to about 80 μm at the sample position. The resultant beam area was unacceptable for subgrain scale investigations, since the grain size was approximately 60μm. Thus, the separation between collimator and sample was subsequently reduced to approximately 8 cm, resulting in an irradiated column approximately 20 μm in diameter.

Beams diffracted from the specimen passed through 3 mm of Al on the front of the image plate holder. A square Pb beam stop was attached to the front of the plate holder (its ''shadow'' can clearly be seen in all of the diffraction patterns). For some of the diffraction patterns, Mo filters were placed in the beam; the resulting sharge change in contrast across the positions within a streak diffracting wavelengths on either side of the K edge [17] was used to identify hkl for the different diffraction streaks and to ensure that (111) streaks were compared for the four samples. Data were initially collected on 20×25 cm image plates with 100 μm pixel size and 1024 levels of contrast, and later on 20×40 cm plates read with 50 μm pixel resolution and 256 levels of contrast. Microtexture was mapped in the specimens by translating the sample along the two orthogonal axes perpendicular to the beam by fixed increments (generally 10 μm) and recording the resulting transmission Laue pattern. More details concerning the technique can be found in [10].

2.1 Experimental Results. Figure 1 compares the transmission Laue patterns from all four specimens, recorded with the smaller sample-collimator separation. The background intensity is white, with darker pixels denoting higher intensities, and the light square near the center of the figures is the shadow cast by the lead beam stop. The black circles mark the ring of azimuthal positions at which diffraction intensity was measured. The contrast between the virgin sample and those with strain histories is evident. The streaks of the virgin sample are very narrow, with little azimuthal broadening evident. By contrast, the strained samples show much broader streaks. The number of peaks is also higher for the strained samples, reflecting the additional texture resulting from the developing microstructure. Also, the presence of distinct ''substreaks,'' closely grouped within a single envelope, is evident, and is more prevalent in the samples with 100% equivalent strain than in the 50% compression sample.

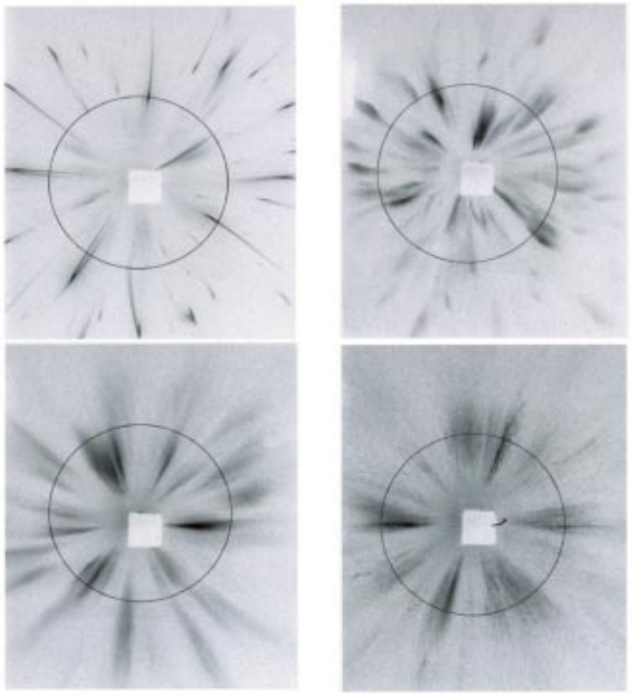

Fig. 1 Transmission Laue patterns recorded with a 10 μm diameter pinhole collimator for as-received OFHC copper, after 50% compression, after 100% torsion, and after 50% compression followed by 50% torsion (clockwise from upper left). Lowest intensities are white with increasing diffraction intensity shown by darker pixels. The light square in each is the beam stop.

The measured azimuthal variation in intensity for the four samples is shown in Fig. 2. Again, there is a clear difference between the virgin sample and the strained samples. The segmented or fragmented peaks support the presence of discrete subregions of the grain, misoriented with respect to the overall crystallographic orientation. The microstructural features are not observed in the virgin sample, and increase as the level of strain

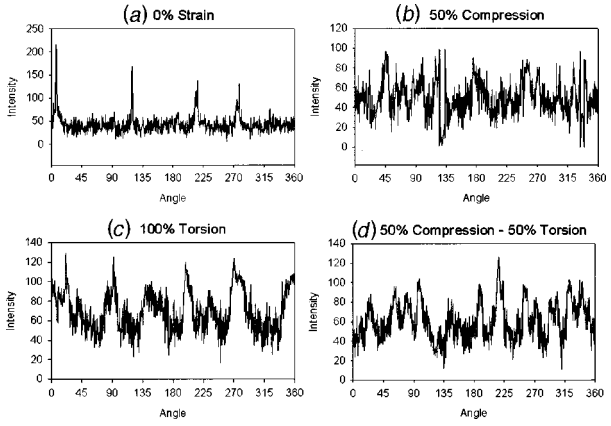

Fig. 2 Azimuthal variation of diffracted intensity along the black circles shown in Fig. 1; strain histories as labeled

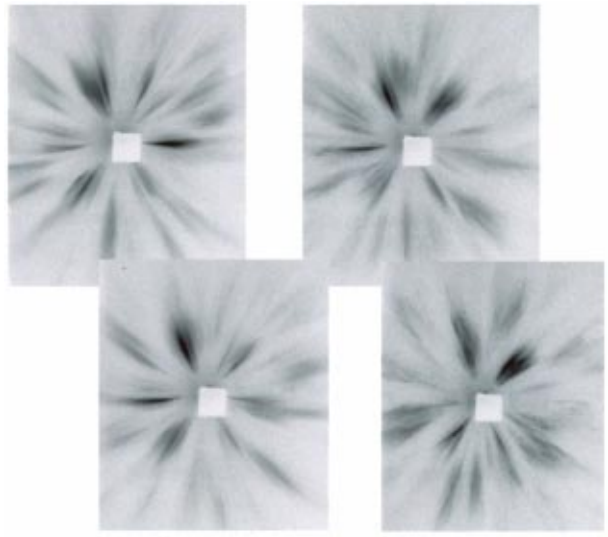

Fig. 3 Laue patterns of the 50% compression, 50% torsion sample at four positions separated by 10 μm translations. The sequence is top left, bottom left, top right, then bottom right.

applied to the material increases. Figure 3 is of the 50% compression, 50% torsion sample and shows diffraction patterns recorded from four positions separated by 10 μm translations. The horizontal diffraction streaks just to the left of the beam stop persist between 10–30 μm; since the maximum beam dimension is between 15 and 20 μm, this demonstrates that the structure observed occurs on a length scale substantially smaller than the original ~60 μm grain size. Also, notice the two patterns of streaks above the beam stop. The group of streaks in the upper left position of the pattern gradually decrease in both intensity and azimuthal range, while those adjacent streaks to the right gradually increase in intensity. The complexity and structural development underlying crystallographic orientations are clearly evident at scales well below the level of the grain.

The electron backscatter work of Hughes and colleagues [8,18–19] resulted in the discovery of scaling laws for key microstructural parameters. For the strain levels considered in this work, high angle GNBs are considered as the dominant source of the misorientation distribution, so we consider a relation for the average misorientation of high angle boundaries within grains which is drawn from their electron backscattering and TEM work. Hughes et al. found that the average angle of misorientation (θ_{av}) between both low angle incidental boundaries and high angle geometrically necessary boundaries (as termed by them) is a function of effective plastic strain. The relations for IBs and GNBs are clearly different; for the high angle GNBs which relate to the higher strain levels considered in the present work,

$$\theta_{av} \propto \overline{\varepsilon^p}^{2/3}, \tag{1}$$

where $\overline{\varepsilon^p} = \sqrt{2/3\varepsilon_{ij}^p \varepsilon_{ij}^p}$ is the equivalent plastic strain. The angle θ_{av} represents a minimum angle between adjacent subgrains determined by considering all cubic symmetry operations for the individual crystallite orientation matrices. The data reported in the present study are consistent with this relationship, as shown in Fig. 4, which shows the measured angular spread (full width) of the (111) diffraction streaks as a function of $\overline{\varepsilon^p}^{2/3}$. Data were taken at well-separated positions (at least one grain diameter apart) from all four samples; the average for all measurements is shown by inverted triangles and, to within experimental scatter, the data follow the prediction of Hughes et al.

The spread of domain orientations is not the only quantity that can be determined; structural variation within individual grains can also be quantified. A sequence of ten Laue patterns recorded

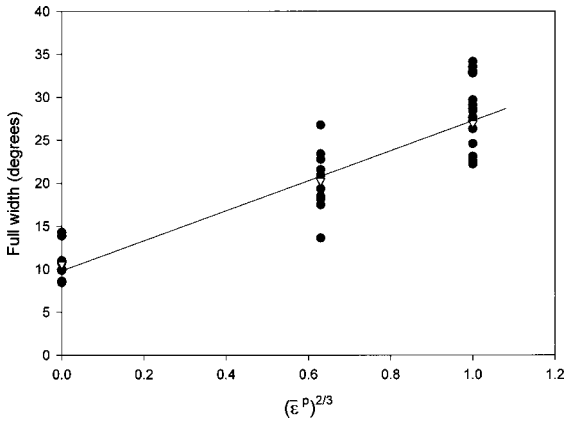

Fig. 4 Variation of angular spread (full width) of streaks from transmission Laue patterns, as a function of $\overline{\varepsilon^p}^{2/3}$. The inverted triangles represent the average width.

after successive 10 μm sample translations illustrates this for a sample strained to 100% in torsion. Again, the azimuthal variation in intensity was measured, and is used to assess the nature of microstructural variation. In this case the intensity from 135 to 215 degrees (measured counterclockwise from vertical) is analyzed, showing the position where a microstructural feature is first detected and its variation with position. Figure 5 shows the measured azimuthal intensity from the first four of the patterns, starting at the sample position 66.94 mm. At the starting position the streak of interest is not detectable (no peak in azimuthal intensity is present). As the sample is translated, a peak in azimuthal intensity begins to form, indicating the presence of a favorably-oriented domain for (111) diffraction. At a sample position of 66.97 mm, this feature is well established. Note that the general shapes of the peaks at positions 66.96 and 66.97 mm are similar, with two lobes or sub-peaks in each case; the intensities are higher at the latter position.

Figure 6 shows the last of the previously measured positions (66.97 mm position), together with the next three positions through 67.00 mm. Of interest is the contrast between the first and subsequent intensity profiles. As discussed in the previous paragraph, there are two well defined sub-peaks evident at sample position 66.97 mm. At higher translations the two sub-peaks are also evident, however the relative intensities have changed; the

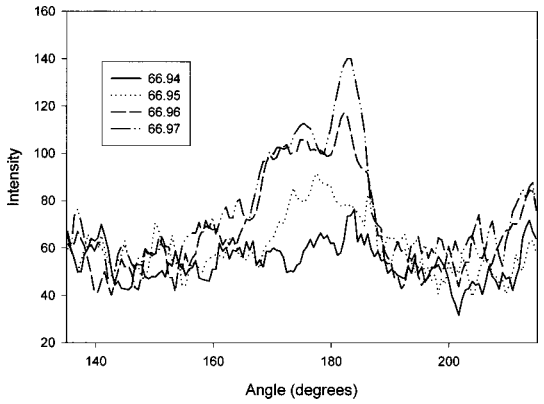

Fig. 5 The variation in measured diffraction intensity at four different sample translation positions (66.94, 66.95, 66.96, and 66.97 mm). The peaks detected at the final two positions indicate the same microstructural feature is within the irradiated cylinder of material.

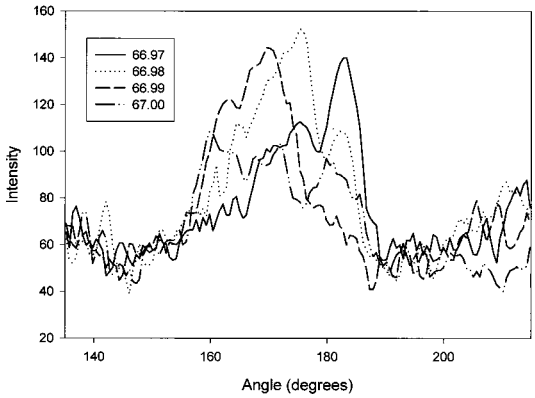

Fig. 6 The variation in measured diffraction intensity at four different sample translation positions (66.97, 66.98, 66.99, and 67.00 mm). The relative sizes of the two subpeaks detected at 66.97 mm and 66.98 mm are reversed.

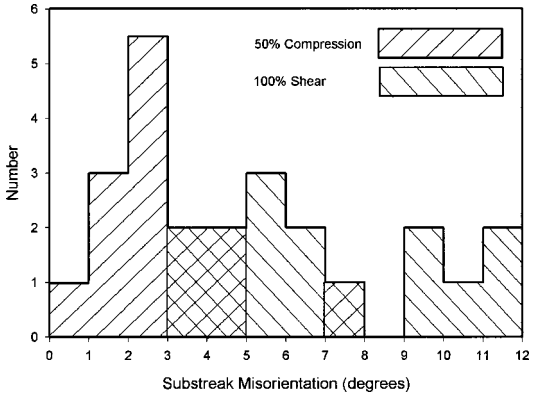

Fig. 8 Histograms for the angular separations between substreaks of a given diffraction streak for the sample which had undergone 50% compression and for the sample subjected to 100% torsion. The five independent measurement positions used were far enough apart to minimize bias.

maximum intensity has changed from the right sub-peak to the left. This sequence implies a region with two subdomains, with differential rotation in the translation direction.

Figure 7 again shows the last of the previous profiles (position 67.00 mm), as well as the next three translations. This figure shows that the microstructural feature prominent in the first position (67.00 mm) has essentially disappeared by the final position (67.03 mm).

Figures 5–7 illustrate the presence of a group of microstructural features of less than 80 μm in size; with an approximate beam size of 20 μm, the size is actually closer to 60 μm. This is consistent with the previously determined grain size. Also illustrated, however, is the fact the changing substructure is clearly visible. There are two clearly observable sub-peaks, and each is predominant in only part of the area in which the streak is produced. The close spatial and orientational correlation of the substreaks of the larger streak indicate that the features are from a single grain, and not from neighboring grains.

Histograms for the angular separations between sub-streaks of a given diffraction streak appear in Fig. 8 for the sample which had undergone 50% compression and for the sample which had been subjected to 100% torsion. The five independent measurement positions used were far enough apart to minimize bias (i.e., the separation was comparable to the grain size in the starting material). The mean, standard deviation and range of angles are 3.2, 1.8, and 7 deg, respectively, for sub-streaks in the 50% compression sample; the values are 7.5, 2.8, and 8 deg, respectively, for the 100% torsion sample. As expected, the sample with greater plastic strain has significantly greater mean misorientation and standard deviation; the fact that the total range of misorientation values observed is more-or-less constant for strains which differ by 50% is most likely a necessary consequence of the combination of domain size, of volume sampled and of the range of wavelengths present in the beam which can penetrate the sample. The picture which emerges from this limited number of measurements is nonetheless consistent with that from the total azimuthal spread of different streaks (Fig. 4) and that from the experimental scaling laws advanced by others [8,18–19].

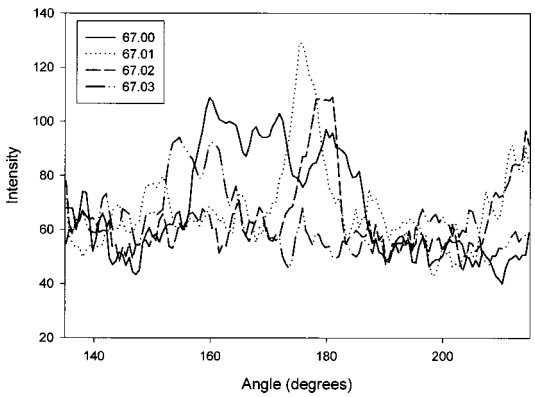

Fig. 7 The variation in measured diffraction intensity at four different sample translation positions (67.00, 67.01, 67.02, and 67.03 mm). At 67.03 mm, the microstructural feature present in the other three patterns is no longer detected.

3 Texture Evolution: Extended Taylor Model With Modified Lattice Spin

Efforts to explicitly account for the subdivision of grains by deformation bands and cells such as that of Leffers [6] are extremely challenging, computationally intensive and inevitably subject to a great deal of idealization of incompletely understood processes and mechanisms. Here we propose a rather simple modification which builds on the earlier suggestions of the work of Butler and McDowell [20] which involves adding an additional term to the lattice spin to represent the diffusion (retardation) of lattice orientation associated with grain subdivision and microtexture formation via deformation bands.

The governing principle for the new term is drawn from a scaling law [8] that relates the average angle of misorientation, θ_{av}, to the average spacing between deformation bands, δ, as per

$$\frac{\delta\theta_{av}}{b} = constant \tag{2}$$

where b is the magnitude of the Burgers vector. Both relations have been verified for a variety of fcc materials.

If $\theta_{av} \propto \overline{\varepsilon}^{p\,2/3}$, then

$$\dot{\theta}_{av} \propto \overline{\varepsilon}^{p\,-1/3}\dot{\overline{\varepsilon}}^{p}. \tag{3}$$

This relation can also be approached from another direction. Combining Eqs. (1) and (2),

$$\delta = A\overline{\varepsilon}^{p\,-2/3};\quad A = \delta_g \overline{\varepsilon}_c^{p\,2/3}, \tag{4}$$

where δ_g is the initial boundary spacing, and $\overline{\varepsilon}_c^p$ allows for the introduction of a threshold effective plastic strain necessary for the onset of microstructural refinement (note that $\delta = \delta_g$ for $\overline{\varepsilon}^p \leq \overline{\varepsilon}_c^p$). Now, define φ, the relative amount of grain subdivision, by

$$\varphi = 1 - \frac{\delta}{\delta_g}. \tag{5}$$

From the similitude relation, normalizing by the initial grain size rather than the Burgers vector magnitude,

$$\left(\frac{\delta}{\delta_g}\right)\theta_{av} = C \tag{6}$$

Since

$$\frac{\dot{\delta}}{\delta_g}\theta_{av} + \frac{\delta}{\delta_g}\dot{\theta}_{av} = 0 \tag{7}$$

this leads to

$$\dot{\theta}_{av} = C\frac{\dot{\varphi}}{(1-\varphi)^2} = \frac{2}{3}C(1-\varphi)^{1/2}\frac{\dot{\bar{\varepsilon}}^p}{\bar{\varepsilon}_c^p} \tag{8}$$

or

$$\dot{\theta}_{av} = \left(\frac{2}{3}C\bar{\varepsilon}_c^{p\,-2/3}\right)\bar{\varepsilon}^{p\,-1/3}\dot{\bar{\varepsilon}}^p. \tag{9}$$

To simplify implementation, one may introduce $\dot{\theta}^*_{av}$, in which the term $2/3C\bar{\varepsilon}_c^{p\,-2/3}$ in Eq. (9) has been divided out, so that

$$\dot{\theta}^*_{av} = \frac{3}{2}C^{-1}\bar{\varepsilon}_c^{p\,2/3}\dot{\theta}_{av} = \sqrt{1-\varphi}\,\bar{\varepsilon}_c^{p\,-1/3}\dot{\bar{\varepsilon}}^p = \bar{\varepsilon}^{p\,-1/3}\dot{\bar{\varepsilon}}^p \tag{10}$$

In view of Eq. (8), we may rewrite this solely in terms of the subdivision variable, i.e.,

$$\dot{\theta}^*_{av} = \frac{3}{2}\frac{\dot{\varphi}}{(1-\varphi)^2}\bar{\varepsilon}_c^{p\,2/3} \tag{11}$$

In the continuum slip theory [21], material is assumed to move though the crystalline lattice via dislocation glide. The lattice structure (with embedded material) undergoes elastic deformations and rigid rotations. The deformation gradient $\mathbf{F}$ is written as

$$\mathbf{F} = \mathbf{F}^*\mathbf{F}^\mathbf{p} = \mathbf{R}\mathbf{U}^\mathbf{e}\mathbf{F}^\mathbf{p} \tag{12}$$

Here, $\mathbf{F}^*$ is associated with the elastic deformation and rigid rotation of the lattice; $\mathbf{F}^\mathbf{p}$ represents the deformation gradient remaining after elastic unloading and after rotating the lattice back to the reference orientation; $\mathbf{R}$ is the lattice rotation tensor and $\mathbf{U}^\mathbf{e}$ is the right elastic stretch tensor. It is understood that $\mathbf{R}$ is comprised of rotation from both elastic deformation and (predominantly) rigid rotation; the former is neglected for small elastic strain. The plastic deformation is described in terms of shearing along crystallographic slip systems. A particular slip system, α, is designated by associated unit vectors $\mathbf{s}_0^{(\alpha)}$ and $\mathbf{m}_0^{(\alpha)}$ for the slip direction and slip plane normal, respectively, in the undeformed lattice; for fcc crystals $\alpha = 1,2,\ldots,12$. These unit vectors are orthonormal in the undeformed lattice and convect with the lattice, so that in the deformed lattice they become

$$\mathbf{s}^{(\alpha)} = \mathbf{F}^*\mathbf{s}_0^{(\alpha)}; \quad \mathbf{m}^{(\alpha)} = \mathbf{m}_0^{(\alpha)}\mathbf{F}^{*-1} \tag{13}$$

These vectors are also orthonormal, but are rotated and stretched with $\mathbf{F}^*$. The velocity gradient $\mathbf{L}$ is given in the current configuration by $\mathbf{L} = \dot{\mathbf{F}}\mathbf{F}^{-1}$, so

$$\mathbf{L} = \dot{\mathbf{R}}\mathbf{R}^\mathrm{T} + \mathbf{R}\dot{\mathbf{U}}^\mathrm{e}\mathbf{U}^{\mathrm{e}\,-1}\mathbf{R}^\mathrm{T} + \mathbf{R}\mathbf{U}^\mathrm{e}\dot{\mathbf{F}}^\mathrm{p}\mathbf{F}^{\mathrm{p}\,-1}\mathbf{U}^{\mathrm{e}\,-1}\mathbf{R}^\mathrm{T} \tag{14}$$

The first two terms involve only rigid lattice rotation and elastic deformation. Separating symmetric and antisymmetric terms,

$$\mathbf{D} = \mathbf{D}^\mathbf{e} + \mathbf{D}^\mathbf{p} + (\mathbf{C}^{*\,-1}\cdot\boldsymbol{\sigma})\mathbf{W}^\mathbf{p} - \mathbf{W}^\mathbf{p}(\mathbf{C}^{*\,-1}\cdot\sigma)$$

$$\mathbf{W} = \dot{\mathbf{R}}\mathbf{R}^\mathbf{T} + \mathbf{W}^\mathbf{e} + \mathbf{W}^\mathbf{p} + (\mathbf{C}^{*\,-1}\cdot\boldsymbol{\sigma})\mathbf{D}^\mathbf{p} - \mathbf{D}^\mathbf{p}(\mathbf{C}^{*\,-1}\cdot\boldsymbol{\sigma}) \tag{15}$$

where $\mathbf{W}^\mathbf{e} = \mathbf{0}$ to first order in elastic strain, and $\mathbf{C}^*$ is the rotated elasticity tensor in the current configuration. The last two terms in each of Eqs. (15) couple the elastic deformation with the plastic rotation (*i.e.*, rotation of the intermediate configuration), albeit typically in a relatively weak manner.

The effect of dislocation substructure formation with its characteristic misorientation distribution following Eq. (2) are introduced by modifying the lattice spin tensor, $\dot{\mathbf{R}}\mathbf{R}^\mathbf{T}$. Since $\mathbf{W} \approx \boldsymbol{\omega} + \mathbf{W}^\mathbf{e} + \mathbf{W}^\mathbf{p}$ where $\omega = \dot{\mathbf{R}}\mathbf{R}^\mathbf{T}$, (then $\omega = \mathbf{W} - \mathbf{W}^\mathbf{p}$), the lattice spin is modified to include a term associated with subgrain/microtexture development, *i.e.*,

$$\boldsymbol{\omega} = \dot{\mathbf{R}}\mathbf{R}^\mathbf{T} = \boldsymbol{\omega}_{sub} = (\mathbf{W} - \mathbf{W}^\mathbf{p})\left(1 + \frac{\beta_w\dot{\theta}^*_{av}}{\|\mathbf{W}^\mathbf{p}\|}\right) \tag{16}$$

where ω_{sub} is the new lattice spin tensor including substructure effects, $\|\mathbf{W}^\mathbf{p}\|$ is the norm of the plastic spin tensor, and $\dot{\theta}^*_{av}$ (rad/s) is the modified rate of change of the average angle of misorientation among sub-grains. The dimensionless coefficient β_w can be adjusted to match experimentally measured texture development. Positive values of β_w tend to increase the rate of texture development; recall that the classical extended Taylor model already overpredicts texture development [16]. Negative values retard texture development, especially during the early stages of plastic deformation. A value of $\beta_w \approx -0.25$ has been found to slow lattice rotations (by roughly a factor of two to five), and leads to preferred orientations in general agreement with measured pole figures. This retardation of lattice rotation can be understood in term of the development of a misorientation distribution of subgrains that are separated by boundaries with significant geometrically necessary dislocation content. Even though the plastic spin is accentuated within each band due to limited activated slip systems (fewer than necessary to fulfill compatibility, in general), there is an alternation of misorientation of the bands so that the net effect is to slow down the average lattice orientation over many bands within a grain. This is clearly demonstrated by traverses of misorientation distribution of the bands (cf. [7]); abrupt changes of misorientation with alternation of sign are observed over traverses of only tens of microns in large strain samples. It is therefore evidently energetically favorable for the geometrically necessary dislocations to be generated in order to accommodate significant local misorientations between bands, while the overall lattice orientation rotates at a significantly lower rate. This lattice spin is assumed to hold for each grain within the context of an extended Taylor assumption which enforces the same deformation gradient $\mathbf{F}$ among all grains in the polycrystalline ensemble [16,20,22].

Predicted results for texture evolution based on the the substructure formulation are next compared with those from the classical ($\omega = \mathbf{W} - \mathbf{W}^\mathbf{p}$ approximation) model and with experimentally measured pole figures for compression. Diffraction intensity measurements were made from modified Lindholm specimens using an automated Phillips Expert system located at the National High Magnetic Field Laboratory at Florida State University. The beam size was 1 mm^2, and the orientation distributions of the (111), (200), and (220) crystal planes were measured. Specimens were mounted in resin, and polished to a smoothness of 1 μm using diamond paste.

Textures (or pole figures) were plotted using the Preferred Orientation Package-Los Alamos, popLA [23]. Measurements were taken at five degree increments in both ϕ (the angle relative to the normal to the surface of the sample) and θ (the angle of rotation about the normal). The outer 10 degrees of each measured pole figure were constructed by routines in popLA, following the procedure described previously [16]. Harmonic analysis was used to extrapolate the high tilt angles, after which the pole figure was re-normalized, to an average overall intensity of 1.00 (times random). The resulting pole figure was then analyzed using the Williams-Imhof-Matthies-Vinel (WIMV) method [24–25], which recalculated the outer ring using the normalization provided by the harmonic analysis. The plane of measurement is normal to the compression axis.

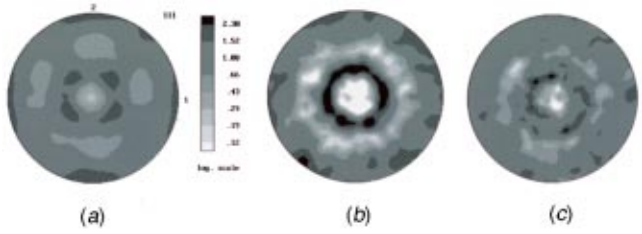

Fig. 9 Comparison of {111} pole figures for OFHC copper following $\bar{\varepsilon}^p = 50\%$ in compression: (*a*) measured, (*b*) calculated based on the classical extended Taylor constraint, and (*c*) calculated based on the non-classical extended Taylor constraint with substructure ($\beta_w = -0.25$).

The predicted pole figures use the model described, both with and without the new substructure terms; in both cases simulations are done with 500 grains based on the extended Taylor assumption of a uniform total deformation gradient in all grains. Individual grain orientations are converted to density files using standard popLA routines and procedures; darker areas in the pole figures correspond to higher orientation densities. The slip system hardening laws and flow rules have been described elsewhere [22], but there is no impact of the slip system hardening law on the texture evolution at large strains because with the extended Taylor model texture evolution is essentially entirely kinematical in nature. Hence, we do not present unnecessary detail. The flow rule is of power law type with a low strain rate sensitivity of 0.01.

Figure 9 shows the stereographs for the transverse specimen face, following compression to 50%. Figure 9(*a*) shows a measured pole figure, which had a maximum intensity of 2.30 times random. Compare this with Fig. 9(*b*), which shows the results of the extended Taylor approximation with no allowance for subgrain microtexture formation. The central void has grown even larger, and the maximal intensity ring is clearly defined. The maximum intensity for this figure is 4.30 times random, a difference of 87% compared to measured. Figure 9(*c*) shows the effect of the substructure modification. Again, the intensities are very similar to those from the measured texture, although there is still a void in the center of the figure, and one area in the outer ring is also noticeably too low. The maximum intensity for this figure was 2.66 times random, a difference of 16% compared to measured, and a reduction of 38% from the results of an extended Taylor simulation with classical lattice spin, $\omega = \mathbf{W} - \mathbf{W}^{\mathbf{p}}$. For the case of torsion, presented in [22], the substructure lattice spin with the same value of $\beta_w = -0.25$ offers even more diffusion of texture relative to the classical formulation.

It is worth pointing out that the use of the extended Taylor assumption with the substructure modification for lattice rotation still undoubtedly overconstrains the kinematics and results in predicted peak intensities that are somewhat too high. Furthermore, it still essentially prescribes Taylor textures; non-ideal components of texture (it asymptotically approaches ideal components), which in reality are associated with the distribution of deformation bands, are not described. Using this substructure model of crystal plasticity in a finite element description for intergranular constraint, for example, might achieve further reductions of texture intensity and might also provide a means of describing variations of microtexture within grains, as an alternative to high degree of freedom, high fidelity models of dislocation substructures with limited active slip systems in each (cf. [6]). In such finite element simulations, non-ideal components of texture would obviously be expected to arise using the present modification of lattice rotation due to departure from the Taylor assumption.

It would appear that gradient models of plasticity which are aimed at reflecting the influence of geometrically necessary dislocation density to accommodate lattice curvature might be of value as a continuum framework [26–28], provided that the length scales of normalization of the gradients are related to the mean spacing of deformation bands over which jumps of lattice orientation occur. In the case of sharp boundaries of deformation bands, presumably dominated by geometrically necessary dislocations, gradient theories of hardening must recognize the discontinuous nature and net orientation of the of the geometrically necessary dislocation population associated with the slab-like volumes of deformation bands [9]. In some cases, the boundaries between deformation bands may be rather less sharp, consisting of dislocation cells of gradually changing orientation over some distance; these so-called transition bands [9] form more diffuse misorientation fields and therefore should alter the length scale for normalization of strain or structure gradients. A viable question to ponder is whether it is the strain gradient or the microstructure gradient that ought to be represented in higher order gradient theories.

Conditions for the possible breakdown of the scaling law in Eq. (2) at very high local shear strains in conjunction with formation of advanced, refined low energy dislocation structures [29] is also of future interest, as are the dependencies of the deformation bands on temperature, strain rate and the presence of second phase particles or precipitates.

4 Conclusions

The results presented demonstrate that microbeam diffraction using polychromatic synchrotron x-radiation can be used to quantify grain subdivision accompanying high levels of deformation in copper. The measured misorientations within grains are consistent with the power law relation with effective plastic strain found by Hughes et al. [8] for GNBs in fcc metals based on entirely different characterization strategies. Results also show that the method can be used to identify the nature and distribution of subdivisions within individual grains.

A simple modification of the lattice rotation is introduced to account for texture retardation due to subdivision. The modification is consistent with the rate of development of the misorientation associated with high angle sub-grain boundaries as expressed by the scaling law of Hughes et al. Extended Taylor simulations for the evolution of crystallographic texture are made for a 500 grain polycrystal, with and without the microstructure effect on lattice spin. Reasonably good agreement with experimental pole figures is shown when the lattice spin is modified to account for sub-grain misorientation distribution.

Acknowledgments

The authors are grateful for the support of the U.S. Army Research Office (AASERT Award DAAG559810213) and the U.S. Office of Naval Research (grants N00014-94-1-0306 and -0726). The experiments were partially performed at SSRL (operated with support of DoE BES). We are grateful to A. Guvenilir, J.D. Haase and Z.U. Rek for their help in collecting microbeam diffraction data. Professor H. Garmestani of Florida State University is thanked for assistance with the texture measurements. D.L. McDowell is grateful for helpful technical discussions on this subject with Dr. Darcy Hughes of Sandia National Laboratories in Livermore, CA.

References

[1] Hansen, N., and Kuhlmann-Wilsdorf, D., 1986, ''Low Energy Dislocation Structures due to Unidirectional Deformation at Low Temperatures,'' Mater. Sci. Eng., **81**, pp. 141–161.
[2] Hansen, N. and Jensen, D. J., 1991, ''Microscopic and Crystallographic Aspects of Flow Stress Anisotropy,'' *Proceedings of Plasticity 1991: The Third International Symposium on Plasticity and Its Current Applications*, Ed. by J.-P. Boehler and A. S. Khan, pp. 131–194.
[3] Kuhlmann-Wilsdorf, D., and Hansen, N., 1991, ''Geometrically Necessary, Incidental, and Subgrain Boundaries,'' Scr. Metall., **25**, pp. 1557–1562.
[4] Hansen, N., and Jensen, D. J., 1992, ''Flow Stress Anisotropy Caused by Geometrically Necessary Boundaries,'' Acta Metall. Mater., **40**, No. 12.
[5] Bay, B., Hansen, N., Hughes, D. A., and Kuhlman-Wilsdorf, D., 1992, ''Evolution of FCC Deformation Structures in Polyslip,'' Acta Metall. Mater., **40**, No. 2, pp. 205–219.

[6] Leffers, T., 1994, ''Lattice Rotations During Plastic Deformation with Grain Subdivision,'' Mater. Sci. Forum, **157–6N**, Part 2, pp. 1815–1820.
[7] Hughes, D. A., 1995, ''The Evolution of Deformation Microstructures and Local Orientations,'' *Proc. 16th Riso Int. Symp. Mat. Sci.*, N. Hansen, D. Juul Jensen, Y. L. Liu, and B. Ralph, eds., pp. 63–85.
[8] Hughes, D. A., Liu, Q., Chrzan, D. C., Hansen, N., 1997, ''Scaling of Microstructural Parameters: Misorientations of Deformation Induced Boundaries,'' Acta Mater., **45**, No. 1, pp. 105–112.
[9] Kuhlmann-Wilsdorf, D., Kulkarni, S. S., Moore, J. T., and Starke, Jr., E. A., 1999, ''Deformation Bands, the LEDS Theory, and Their Importance in Texture Development: Part I. Previous Evidence and New Observations,'' Metall. Mater. Trans. A, **30A**, pp. 2491–2501.
[10] Guvenilir, A., Butler, G. C., Haase, J. D., McDowell, D. L., and Stock, S. R., 1998, ''X-ray Microbeam Quantification of Grain Subdivision Accompanying Large Deformations of Copper,'' Acta Mater., **46**, No. 18, pp. 6599–6604.
[11] Patterson, II, C. R., Ignatiev, K. I., Guvenilir, A, Haase, J. D., Morano, R., Rek, Z. U., and Stock, S. R., 2000, ''Nondestructive Determination of the Depth of Different Texture Components in Polycrystalline Samples,'' *Proc. Mater. Res. Soc.*, Vol. 590, pp. 253–258.
[12] Juul Jensen, D., Kvick, A., Lauridsen, E. M., Lienert, U., Margulies, L, Nielsen, S. F. and Poulsen, H. F., 2000, ''Plastic Deformation and Recrystallization Studied by the 3-D X-ray Microscope,'' *Proc. Mater. Res. Soc.*, Vol. 590, pp. 227–240.
[13] Lienert, U., Martins, R., Grigull, S., Pinkerton, M., Poulsen, H. F. and Kvick, A., 2000, ''High Spatial Resolution Strain Measurements with Bulk Materials by Slit-Imaging,'' *Proc. Mater. Res. Soc.*, Vol. 590, pp. 241–246.
[14] Larson, B. C., Tamura, N., Chung, J.-S., Ice, G. E., Budai, J. D., Tischler, J. Z., Yang, W., Weiland, H., and Lowe, W. P., 2000, ''3-D Measurement of Deformation Microstructure in Al(0.2%)Mg using Submicron Resolution White X-ray Microbeams,'' *Proc. Mater. Res. Soc.*, Vol. 590, pp. 247–252.
[15] Graham, S., 1995, ''The Stress State Dependence of Finite Inelastic Deformation Behavior of FCC Polycrystalline Materials,'' Master's thesis, GWW School of Mechanical Engineering, Georgia Institute of Technology, Atlanta, GA.
[16] Butler, G. C., Graham, S., McDowell, D. L., Stock, S. R., and Ferney, V. C., 1998, ''Application of the Taylor Polycrystal Plasticity Model to Complex Deformation Experiments,'' ASME J. Eng. Mater. Technol., **120**, pp. 197–205.
[17] Stock, S. R., Rek, Z. U., Chung, Y. H., Huang, P. C., and Ditchek, B. M., 1993, J. Appl. Phys., **73**, pp. 1737–1742.
[18] Campbell, G. H., Foiles, S. M., Huang, H., Hughes, D. A., King, W. E., Lassila, D. H., Nikkel, D. J., de la Rubia, T. D., Shu, J. Y., Smyshlyaev, V. P., 1998, ''Multi-scale Modeling of Polycrystal Plasticity: A Workshop Report,'' Mater. Sci. Eng., A, **251**, pp. 1–22.
[19] Godfrey, A. and Hughes, D. A., 1998, ''Characterization of Dislocation Wall Spacing Distributions,'' Proceedings of the 1998 TMS Annual Meeting, pp. 191–199.
[20] Butler, G. C., and McDowell, D. L., 1998, ''Polycrystal Constraint and Grain Subdivision,'' Int. J. Plast., **14**, No. 8, pp. 703–717.
[21] Asaro, R. J., 1983, ''Crystal Plasticity,'' ASME J. Appl. Mech., **50**, pp. 921–934.
[22] Butler, G. C., 1999, ''Incorporation of Dislocation Substructure into Crystal Plasticity Theory,'' Ph.D. thesis, GWW School of Mechanical Engineering, Georgia Institute of Technology, Atlanta, GA.
[23] Kocks, U. F., Kallend, J. S., Wenk, H.-R., Rollett, A. D., Wright, S. I., 1994. *Preferred Orientation Package—Los Alamos*. Document LA-CC-89-18, Los Alamos National Laboratory.
[24] Matthies, S., 1982, ''Form Effects in the Description of the Orientation Distribution Function (ODF) of Texturized Materials by Model Components,'' Phys. Status Solidi B, **112**, pp. 705–716.
[25] Wenk, H.-R., 1985, *Preferred Orientation in Deformed Metals and Rocks: An Introduction to Modern Texture Analysis*, Academic Press, NY.
[26] Zbib, H. M., and Aifantis, E. C., 1992, ''On the Gradient-Dependent Theory of Plasticity and Shear Banding,'' Acta Mech., **92**, pp. 209–225.
[27] Fleck, N. A., and Hutchinson, J. W., 1993, ''A Phenomenological Theory for Strain Gradient Effects in Plasticity,'' J. Mech. Phys. Solids, **41**, No. 12, pp. 1825–1857.
[28] Fleck, N. A., Muller, G. M., Ashby, M. F., and Hutchinson, J. W., 1994, ''Strain Gradient Plasticity: Theory and Experiment,'' Acta Metall. Mater., **42**, pp. 475–487.
[29] Kuhlmann-Wilsdorf, D., 1989, ''Theory of Plastic Deformation: Properties of Low Energy Dislocation Structures,'' Mater. Sci. Eng., **A113**, pp. 1–41.